Regulation of degenerative spheroids after injury

Yu Yong
University of Virginia
Kanchana Gamage
Harvard University
Courtny Cushman
University of Virginia
Anthony Spano
University of Virginia
Christopher D Deppmann (deppmann@virginia.edu)
University of Virginia https://orcid.org/0000-0002-6591-1767

Research article

Keywords: Axonal spheroids; Wallerian degeneration; NAD+; DR6; SARM1; WLDs; membrane rupture; Rho activation

Posted Date: May 7th, 2020

DOI: https://doi.org/10.21203/rs.3.rs-26384/v1

Abstract

Background Neuronal injury leads to rapid, programmed disintegration of axons distal to the site of lesion. Much like other forms of axon degeneration (e.g. developmental pruning, toxic insult from neurodegenerative disorder), Wallerian degeneration associated with injury is preceded by spheroid formation along axons. The mechanisms by which injury leads to formation of spheroids remains elusive. Methods Here, using wild-type and mutant neonatal mouse primary sympathetic neurons, immunostaining and calcium imaging, we investigate the roles of players previously implicated in the progression of Wallerian degeneration in injury-induced spheroid formation. Results We find that intra-axonal calcium flux is accompanied by actin-Rho dependent growth of calcium rich axonal spheroids that eventually rupture, releasing material to the extracellular space prior to catastrophic axon degeneration. Importantly, after injury, Sarm1 -/- and DR6 -/- , but not Wld s (excess NAD +) neurons, are capable of forming spheroids that eventually rupture, releasing their contents to the extracellular space. Supplementation of exogenous NAD + or expressing WLD s suppresses Rho-dependent spheroid formation and degeneration in response to injury. Conclusions Taken together, our findings place Rho-actin and NAD + upstream of spheroid formation and may suggest that other mediators of degeneration, such as DR6 and SARM1, mediate post-spheroid rupture events that lead to catastrophic axon disassembly.

Background

Axons are the primary information conduits of the nervous system. Failure to maintain the integrity of axons is a feature of many neurological disorders. In response to injury, a process of axonal fragmentation, or Wallerian degeneration (WD) occurs, often resulting in permanent loss of neural function [1]. Immediately after injury, the severed axon goes through a latent phase where its overall morphology remains unchanged for 1–2 hours *in vitro* and up to 48 hours *in vivo* [2, 3]. Intracellular calcium increases transiently during the latent phase, followed by a second global calcium wave just prior to axon fragmentation [4]. Elevation of intracellular calcium through L-type calcium channels and sodium-calcium exchanger (NCX), together with impaired mitochondrial motility and calcium buffering capacity, results in activation of the calpain protease and irreversible disassembly of the axon [5–10]. In addition to calcium flux, severed axons display cessation of axonal transport, formation of axonal swellings, fragmentation of neurofilaments and removal of debris by recruited phagocytes. This rapid and near synchronous axonal disintegration period is called the catastrophic/execution phase of degeneration and beyond injury can be observed in developmental and other pathological regressive contexts [11–13].

Our first insight into the non-passive nature of WD signaling came from the *Wld*^{S} mouse which harbors a neomorphic gain of function mutation and displays axon degeneration that is 10 times slower after injury compared to wild-type neurons [14, 15]. The *Wld*^{S} gene encodes a chimeric fusion protein, consisting of the full-length nicotinamide mononucleotide adenyltransferase 1 (NMNAT1), which synthesizes NAD^{+} from its substrate nicotinamide mononucleotide (NMN), and a fragment of the ubiquitination factor

UBE4B [16]. The perdurance of high NAD^+ levels in axons is sufficient to delay Wallerian degeneration [17]. As such, depletion of NAD^+ is known to be an important trigger for WD and is achieved in several ways after injury: **1**. Turnover of NMNAT2 regulated by the ubiquitin proteasome system (UPS), palmitoylation of cysteines in NMNAT2 and mitogen-activated protein kinase (MAPK) signaling [18–21] and **2**. Activation of sterile alpha and armadillo motif (SARM1), which has intrinsic NAD^+ cleavage activity [22–24]. Beyond proteins that influence NAD^+ levels, several other factors have been implicated in promoting Wallerian degeneration including death receptor 6 (DR6), calpain, Phr1 E3 ubiquitin ligase, dual leucine zipper kinase (DLK), c-jun n-terminal kinase (JNK), and axundead (Axed) [6, 25–31]. Whether these factors all converge on similar signaling hubs such as NAD^+ remains to be determined.

Formation and growth of axonal spheroids has been identified in various models of degeneration, including optic nerve injury, Alzheimer's disease, Parkinson's disease and amyotrophic lateral sclerosis [13, 32, 33]. Recently, we found that these spheroids are not merely a morphological hallmark of degeneration induced by trophic withdrawal but are also functionally consequential, mediating the transition from latent to catastrophic phase [10]. Despite a good amount of descriptive information about the content of these spheroids [13, 34], whether they are regulated by the aforementioned players, NMNATs, SARM1, or DR6, remains unresolved.

Here, we demonstrate that prior to catastrophic degeneration, intra-axonal calcium increases and decreases corresponding to growth and rupture of axonal spheroids. We further demonstrate that Rho activation and changes to the actin cytoskeleton are both required for spheroid formation after injury. Finally, we find that after injury, neurons derived from *Wld*^{S} mice display impaired spheroid formation and rupture. We show that upstream of Rho activation, both exogenous supplementation of NAD^+ and the presence of a more stable axonally targeted NMNAT, such as WLD^S, suppress spheroid formation. In contrast, loss of *DR6* or *SARM1* has minimal effect on spheroid formation and rupture after injury. These findings indicate a separable role of classic Wallerian degeneration effectors with respect to spheroid formation after axotomy.

Methods

Chemicals and reagents

Fluo-4 (F14200), Fluo-4 AM (F14201), Dextran Texas Red, 3,000, 10,000, and 70,000 MW (D3329, D1828, and D1830, respectively) were purchased from Thermo Fisher Scientific. CT04 and CN03 were the products of Cytoskeleton Inc. Cytochalasin D (C2618), cytosine arabinofuranoside (Ara-C), poly-D-lysine, and paraformaldehyde were purchased from Millipore Sigma. NGF was purified from mouse salivary glands. Goat anti-mouse Alexa 488, 10% goat serum, and laminin (1 µg/mL) were products of Life Technologies. Mouse Tuj1 primary antibody was the product of Covance. DMEM high glucose (11965092), DMEM/F-12 (11320033), DMEM/F-12 phenol red free (21041025), DMEM high glucose,

calcium free (21068028), 100X penicillin/streptomycin (10378016), and FBS (16000044) were brought from Gibco.

Animals

All experiments were carried out in compliance with the Association for Assessment of Laboratory Animal Care policies and approved by the University of Virginia Animal Care and Use Committee. All mice were on a C57BL/6J.129S mixed background except for *Wld*^{S} mice, which were FVB/NJ background. *Wld*^{S} and *Sarm1*$^{-/-}$ animals were purchased from the Jackson labs. *DR6*$^{-/-}$ animals were a generous gift from Genentech. Males and females were mixed in all experiments.

Primary Sympathetic neuronal cultures

Sympathetic neuron cultures were established as described previously [35]. Briefly, neurons were obtained by dissociation of P0-P2 mouse superior cervical ganglia. These neurons (from each litter of pups) were plated in compartmentalized microfluidic devices coated with poly-D-lysine (50 μg/mL) and laminin (1 μg/mL) in DMEM supplemented with 10% FBS, penicillin/streptomycin (1U/mL), and 45 ng/mL of NGF at 37^{0}C. Glial cells were removed from cultures using 5 μM Ara-C for 48–72 hours.

Axotomy experiments in vitro

Neurons from each litter of pups were allowed to project their axons to the axonal chamber (3–7 DIV) after plating. After the axons had grown into the axonal chamber, neurons were enucleated by aspirating 3 mL of 1x PBS through the cell body chamber leaving the axons intact in their respective chamber. Unless otherwise indicated, both compartments were replaced with DMEM supplemented with 10% FBS, penicillin/streptomycin (1U/mL) and 45 ng/mL of NGF and incubated at 37^{0}C and 10% CO_2 for indicated times.

Immunocytochemistry

Immunocytochemistry was carried out as previously described [36]. Briefly, at the indicated times, axons were fixed in 4% paraformaldehyde (w/v)/ phosphate buffered saline (PBS) at room temperature for 20 minutes, washed 3 × 5 min with 1x PBS, and blocked/permeabilized (5% goat serum, 0.05% Triton-x-100 in PBS) for 1 hour at room temperature. Axons were then incubated overnight at 4^{0}C with primary antibody diluted in the blocking buffer. Cells were then washed 3 × 5 min with 1x PBS and incubated with fluorescent secondary antibody for 1 hour at room temperature. Cells were again washed with 1x PBS three times and imaged using a fluorescent inverted microscope. All *in vitro* experiments were performed in triplicate with at least two microfluidic devices used for each condition.

Live imaging

Sympathetic neuron cultures were washed 3 times with DMEM/F-12, phenol red free, and incubated for 30 minutes at 37^{0}C and 10% CO_2 with live imaging dyes diluted in DMEM/F-12, phenol red free. Cells were then imaged under Leica SP5 X confocal microscope in W.M. Keck Center at the University of

Virginia. Axons in grooves of the microfluidic chamber were imaged after injury. For membrane rupture, dextran dyes diluted in DMEM/F-12, phenol red free were added to the microfluidic chamber 20 minutes after injury.

Image Processing and analysis

Axon degeneration in culture was quantified from β3-tubulin stained fluorescence images by counting the number of individual axons at the leading edge that had at least three beads/blebs as described [26]. A blinded investigator counted ten representative pictures of the axons, in two microfluidic chambers per condition/time point. On each image 10 50 µm boxes were randomly assigned to single axons. The investigator took care not to box bundles of axons, which may confound analysis. Then the number of boxes, which had 3 or more beads/blebs were counted and categorized as degenerating axons. Equal to or more than 80% degeneration was considered maximum degeneration and equal to or less than 10% degeneration of axons was considered as minimum degeneration. The percentage of the total number of degenerating axons was calculated using Microsoft Excel. At least 300 total axons were counted for each condition. The standard error of the mean was considered as error. In live imaging, Ca^{2+} intensity (ΔF/F0), the size (S/S0) and number of axonal spheroids were quantified in selected ROI (single axon or axonal spheroid) by Fiji software [37]. Each experiment was repeated at least 3 times with separate litters of mouse pups of the same genotype.

Calcium measurement

Conditioned media was diluted in milliQ water (1:20) and mixed thoroughly. 100µL of reaction mixture was made with 1µL HEPES, 2µL 1 mM Fluo-4 (20 mM working concentration), 10µL diluted conditioned media, and 87µL water. Black 96 well plate was used in Spectrophotometric assay. Eight $CaCl_2$ standards (2.54 µM, 4.87 µM, 9.75 µM, 19.5 µM, 39 µM, 78 µM, 156 µM, and 313 µM) were used to calculate a standard curve for analyzing Ca^{2+} concentration in conditioned media.

Statistics

Statistical analysis was performed in Prism 8.0 software (GraphPad). All measurements are shown as mean ± SEM. For samples defined by one factor, data were compared by unpaired two-tailed *t* tests for two samples or one-way ANOVA with Tukey's *post hoc* multiple comparisons test for three or more samples. For samples defined by two factors, data were compared by two-way ANOVA with Sidak's or Dunnett's *post hoc* multiple comparisons test. Sample size (n) was defined as the number of axons or axonal spheroids counted in the live imaging experiment, or the number of independent cultures that were quantified in each experiment. The null hypothesis was rejected at the 0.05 level. *P* values < 0.05 were considered significant and represented by asterisks. The statistical test, sample size (n), and the *p* values were reported in the figure legends.

Results

Intra-axonal calcium increases in enucleated axons and accumulates in spheroids prior to catastrophic degeneration

We first sought to determine whether calcium accumulates in spheroids after injury as we have observed previously for degeneration associated with trophic deprivation. To this end, we cultured mouse sympathetic neurons in microfluidic devices, which separate soma and axons (Fig. 1A). Cell bodies of sympathetic neurons were enucleated by aspiration of the cell body chamber in PBS, which leaves axons residing in the distal axon chamber and microgrooves intact. After injury, these axons remain intact for roughly an hour as measured by microtubule integrity (β3-tubulin staining). At the conclusion of the latent phase, the majority of axons rapidly degenerate, going from 7.5 ± 2.08% to 82.75 ± 3.9% of degeneration within 90 minutes (Fig. 1B,C). This is referred to as the catastrophic or execution phase of degeneration [38]. At the transition between latent and catastrophic phases: 0 to 90 minutes for injury, we applied the Fluo4-AM calcium dye to axons 30 minutes prior to imaging (Fig. 1D). For injured axons, intra-axonal calcium had a roughly 2-fold increase from baseline prior to onset of the catastrophic phase (Fig. 1E). Much of this calcium was concentrated in nascent spheroids (Fig. 1D), consistent with previous *in vivo* and *in vitro* injury studies [34, 39] and similar to our recent findings in the context of trophic withdrawal [10]. After observing the initial formation of calcium rich spheroids, these structures increase in size from 3.2 ± 0.4μm^2 to 13 ± 1.2μm^2 (roughly 400%) between 20 and 80 minutes after injury. Spheroidal calcium levels increased by roughly 5-fold at 1 hour after injury (Fig. 1G). Interestingly, spheroidal calcium levels decrease as spheroids increase in size. Besides the increase in size and calcium level in individual spheroids, the number of spheroids increased from 0.54 ± 0.14 to 6.8 ± 0.53 per 100 μm of axon between 5 and 60 minutes after injury (Fig. 1F). We also examined spheroidal calcium as a function of spheroidal area and found the same trend (Fig. 1H). Taken together, these results indicate that the formation of calcium rich axonal spheroids is a morphological hallmark that occurs prior to entry into the catastrophic phase of degeneration after injury.

Formation of axonal spheroids requires Rho activity and actin remodeling

What signaling pathways trigger axonal spheroid formation after injury? Given the dramatic outgrowth of membrane, we speculated that spheroid formation may involve cytoskeletal remodeling, similar to what we observed after trophic deprivation [10]. To examine actin and β3-tubulin abundance in spheroids we stained enucleated axons with phalloidin 1 hour after injury. We found that actin accumulated in 47.5 ± 3.9% of the spheroids examined, while β3-tubulin accumulated in 32.1 ± 4.4% of spheroids (Fig. 2A). We next sought to determine whether actin remodeling is required for spheroid formation. To examine this, cultures were pre-treated (3hrs prior to injury) with the actin polymerization inhibitor cytochalasin D (10 μg/μL), which delayed spheroid formation (Fig. 2B,C). Rho activation is known to influence actin assembly [40], and may serve as a molecular switch to govern spheroid formation. Indeed, inhibiting Rho family members using the C3 transferase, CT04 (1 μg/mL, 2hrs prior to injury), also suppressed spheroid formation (Fig. 2B,C). Interestingly, pretreatment with cytochalasin D or CT04 delayed degeneration for up to 4 hours after injury (Fig. 2D,E).

Axonal spheroids develop membrane rupture after injury

We and others have shown that the electrical chemical gradient can be disrupted through membrane rupture on axonal spheroids in models of developmental degeneration and multiple sclerosis [10, 41]. To determine whether the axonal spheroids that we observed on injured sympathetic axons develop ruptures, we bathed axons in neutral fluorescent dextran beginning 20 minutes after injury, which is sufficient time for the initial site of lesion to re-seal [42]. If there were any ruptures on the membrane after injury, the 3 kDa red dextran would immediately diffuse to the axoplasm (Fig. 3A). As expected, the exclusion of dextran was maintained for 40–50 minutes after injury, however after 50 minutes, the axoplasm begins to fill with fluorescent dextran (Fig. 3B). An additional movie file shows the dextran filling up axonal spheroids in more detail [see Additional file 1]. We also examined the size of ruptures using different sized dextrans. We observed that 70, 10, and 3 kDa dextran filled 11.5 ± 2.6%, 33 ± 6.6% and 63.6 ± 7.1% of axonal spheroids by 90 minutes after injury, respectively (Fig. 3C). This indicates permeability of small to medium sized molecules and suggests the same physiology of spheroidal rupture in WD as other degeneration paradigms. To determine whether dextran diffusion correlates with the size of spheroids, we counted the numbers and sizes of 3 kDa dextran positive and negative spheroids 30, 60, and 90 minutes after injury, respectively (Fig. 3D). Most of the axonal spheroids are 5–10μm^2 in size. However, regardless of their sizes, more spheroids develop membrane rupture at later times after injury suggesting that the probability of rupture is more impacted by time than size of spheroid.

Based on the diminution of spheroidal calcium signal 1 hour after injury and the permeability of the spheroidal membrane, we speculate that intra-axonal calcium may diffuse to the extracellular space after spheroidal rupture. To test this hypothesis, we bathed axons in microfluidic devices in 100μL of regular culture media or calcium free, serum free media and measured extracellular calcium before and 1 hour after injury using a Fluo4 spectrophotometric assay [10]. For the cultures maintained in regular SCG media, calcium levels in conditioned media taken from injured axons (ICM) (2409.51 ± 212.17 μM) was significantly higher than calcium concentration in Control CM (1578.16 ± 275.57 μM) (Fig. 3E). Additionally, we were able to observe an increase in extracellular calcium after spheroidal rupture when experiments were performed using calcium free, FBS free media (Fig. 3E). Whether or not this calcium extrusion is physiologically relevant remains to be determined. However, in this *in vitro* system it represents a complementary paradigm to the aforementioned dextran assay for assessing membrane integrity.

Spheroid formation in WD deficient mutants

We next examined the spheroid formation in genotypes reported to have impaired Wallerian degeneration: *Wld^S*, *DR6$^{-/-}$* and *Sarm1$^{-/-}$*. Calcium imaging revealed that *Wld^S* did not display a late stage calcium wave, and had a greatly diminished capacity to form spheroids in response to injury (Fig. 4A,B). This is consistent with previous observations demonstrating that mitochondria in *Wld^S* neurons have increased calcium buffering capacity and a delay in spheroid formation [4, 5, 7, 34]. Interestingly, neurons from *DR6$^{-/-}$* and *Sarm1$^{-/-}$* mice also had attenuated spheroidal calcium compared to wild-type but

significantly higher than *Wld*^{S} neurons (Fig. 4B). We next examined the role of WLD^S, DR6 and SARM1 in the change in spheroid size and the accumulation of spheroids as a function of time after injury. 1 hour after injury, we observed that loss of *DR6* or *SARM1* displayed a roughly 100% increase in spheroid size (Fig. 4C). Moreover, wild-type, *DR6*$^{-/-}$, and *Sarm1*$^{-/-}$ neurons displayed 7.5 ± 0.8, 9.1 ± 0.5, and 9.7 ± 0.7 spheroids per 100 µm of axons, respectively, whereas *Wld*^{S} neurons only displayed 1.4 ± 0.5 spheroids per 100 µm of axons 1 hour after injury (Fig. 4D). We next examined spheroid rupture and calcium extrusion in sympathetic axons from *Wld*^{S}, *DR6*$^{-/-}$ and *Sarm1*$^{-/-}$ mice. WT, *DR6*$^{-/-}$ and *Sarm1*$^{-/-}$ all displayed similar levels of 3 kDa dextran spheroid filling after injury, however *Wld*^{S} axons displayed negligible filling indicating a lack of spheroid rupture (Fig. 4E,F). Consistent with this, *Wld*^{S} axons showed no difference in extracellular calcium levels before or 1 hour after injury, while *DR6*$^{-/-}$ and *Sarm1*$^{-/-}$ displayed elevation in extracellular calcium levels (Fig. 4G). Taken together, these findings suggest that WLD^S/NMNAT is upstream of spheroid formation while the other players tested have minimal roles in this process.

NAD $^+$ acts upstream of Rho activation to suppress spheroid formation

The Wld^S protein stably targets NMNAT1 to axons to maintain high NAD$^+$ levels for prolonged periods following injury, which is known to protect axons from degeneration [43]. To test whether NAD$^+$ contributes to the formation of axonal spheroids, we treated sympathetic axons with 1 mM exogenous NAD$^+$ overnight prior to injury. Supplementation of NAD$^+$ to wild-type sympathetic axons suppressed spheroid formation after injury (Fig. 5A,B), and phenocopied observations in *Wld*^{S} axons (Fig. 4A,D). We next examined whether NAD$^+$ is upstream of Rho activation with respect to regulating spheroid formation. To this end, axons were incubated with the Rho activator, CN03 in the presence of exogenouse NAD$^+$. Interestingly, activation of Rho was able to promote spheroid formation even in the presence of exogenous NAD$^+$ (Fig. 5A,B), suggesting that high NAD$^+$ levels inhibit Rho thereby preventing spheroid formation. NAD$^+$ levels are known to decline in injured axons and nerves, due to both turnover of NMNAT2 and SARM1-dependent NAD$^+$ degradation [18, 44, 45]. However, loss of *SARM1* failed to inhibit spheroid formation, whereas *Sarm1*$^{-/-}$ neurons pre-treated with NAD$^+$ or Rho inhibitor CT04 displayed only 1.16 ± 0.52 and 0.85 ± 0.31 spheroids per 100 µm of axons 1 hour after injury, respectively (Fig. 5C,D). Moreover, activation of Rho by CN03 in *Wld*^{S} neurons increased the number of spheroids to 3.59 ± 0.87 per 100 µm of axons 1 hour after injury (Fig. 5E,F). We further examined the protection effects of NAD$^+$ in the presence and absence of Rho activation. 4 hours after injury wild-type sympathetic axons treated with exogenous NAD$^+$ remained intact, but degeneration was partially rescued (41.7 ± 0.3%) by CN03 incubation (Fig. 5G,H). 8 hours after injury, *Wld*^{S} axons treated with CN03 displayed 60.5 ± 3.4% degeneration, significantly higher than control *Wld*^{S} cultures with 13.8 ± 7.1% degeneration (Fig. 5G,H).

Discussion

Here we describe the regulated formation of calcium rich axonal spheroids as injured axons transition from latent phase to catastrophic degeneration. Importantly, among three WD deficient mutants, only

Wld^{S} suppresses spheroid formation, suggesting that depletion of axonal NMNAT/NAD^{+} acts upstream of spheroid formation during the latent phase, whereas SARM1 and DR6 activation might promote degeneration during catastrophic phase (Fig. 6). This is somewhat surprising given that the mechanism of SARM1 action is thought to be through NAD^{+} degradation [23, 24]. This sets up a scenario whereby NAD^{+} may be acting at different points in the degeneration timeline after injury. It is known that the initial decay of NAD^{+} after injury is independent of SARM1 and we suggest that this reduction is sufficient for the disinhibition of Rho induced spheroid formation. After spheroid rupture, we suggest that DR6 and SARM1 are activated by an as yet unknown mechanism to further drive down the level of NAD^{+} and promote catastrophic axon degeneration (Fig. 6).

Axonal spheroids have been characterized as a common morphological hallmark during axon degeneration [13]. These spheroids arise continuously in axons and show different degrees of swelling in response to a range of molecular triggers, including the focal blockage of axonal transport, ROS mediated actin aggregation, and NMNAT deficiency [32, 33, 39]. Here, we report the formation of calcium rich spheroids on severed sympathetic axons *in vitro* (Fig. 1). Similar to our observations in developmental degeneration models [10], we find that spheroid formation requires Rho dependent actin remodeling. Inhibition of this pathway not only blocked spheroid formation but also delayed injury induced degeneration (Fig. 2).

By comparing axoplasmic calcium dynamics of WD deficient mutants with wild-type sympathetic axons, we demonstrated that neurons from *Wld*^{S} animals display minimal axonal calcium flux from 20 to 90 minutes after injury, significantly fewer and smaller axonal spheroids formed, and no calcium extrusion to the extracellular space (Fig. 4). These findings suggest that injury induced NMNAT depletion is likely an upstream trigger for calcium rich spheroid formation and rupture. SARM1 has been proposed to be in the same pathway as Wld^{S}/NMNAT1 in promoting axon degeneration due to its intrinsic NAD^{+} cleavage activity [23, 24, 46, 47]. Surprisingly, unlike *Wld*^{S}, *Sarm1*$^{-/-}$ axons are capable of forming axonal spheroids after injury suggesting that at least in the context of spheroid formation and rupture, these pathways operate independently. Importantly, this finding is not in conflict with reports that NMNAT/NAD^{+} depletion is involved in catastrophic degeneration [45]. Studies in mouse dorsal root ganglion (DRG) neuron cultures have shown that there is slow NAD^{+} decline for roughly 2 hours after transection likely owing to NMNAT2 degradation, followed by a fast SARM1-dependent NAD^{+} degradation [44, 45, 48]. To explain the different phenotypes of *Sarm1*$^{-/-}$ and *Wld*^{S} with respect to spheroid formation after injury, we propose a working model by which SARM1 is inactive during the latent phase and then becomes active after spheroidal rupture to accelerate NAD^{+} depletion during the catastrophic phase of axon degeneration.

The mechanism by which NAD^{+} inhibits Rho activity and spheroid formation remains unknown and will be the subject of future inquiry. We envision a few possibilities: **1**. The replenished axonal NAD^{+} pool might inhibit the calcium release from intracellular stores, which contributes to the formation of calcium enriched spheroids. NAD^{+} depletion after injury leads to the increase of relative concentrations of

calcium-mobilizing agents including cADPR and ADPR over axonal NAD^+, stimulating intra-axonal calcium rise by activation of ryanodine receptors on ER and calcium channels on plasma membrane, respectively [49]. In addition, blocking ER calcium channels has been shown to protect injury-induced axonal degeneration in DRG cultures and secondary degeneration of severed CNS axons [50, 51]. However, whether blocking intracellular calcium stores would suppress spheroid formation on injured sympathetic axons must be investigated in the future. **2**. Depletion of NAD^+ pools after injury alters axonal redox state and ATP synthesis [52] which may contribute to spheroid formation and rupture by regulating Rho GTPase activity (Fig. 6). Studies have shown that the cellular oxidation state mediates activation of Rho GTPase via a redox-sensitive cysteine at the end of p-loop motif [53, 54]. Moreover, application of Rho activator CN03 was able to promote spheroid formation on injured axons in the presence of NAD^+ supplementation (Fig. 5A,B). The disruption of redox state or NAD^+/NADH balance caused by NMNAT degradation may therefore activate Rho to mediate actin remodeling and spheroid formation.

The mechanism by which SARM1 is activated after spheroid rupture remains unclear, but the recent finding that NMN analogue can activate SARM1 to induce non-apoptotic cell death appears to provide one possible answer to this question [55]. Activation of SARM1 has been shown to promote phosphorylation of JNK to trigger neuronal immune response after axonal injury [56]. Moreover, phosphorylation of SARM1 by JNK regulates NAD^+ cleavage to inhibit mitochondrial respiration in response to oxidative stress [30]. Therefore, SARM1 may also be activated by JNK to promote further NAD^+ depletion (Fig. 6). Both overexpression of NMNATs and knocking out SARM1 have been shown to decrease injury-induced degradation of the calpain inhibitor, calpastatin, which protects neurons from degeneration [8, 57]. It is possible that NAD^+ depletion and further energy deficits lead to calpastatin degradation, which would disinhibit calpain to promote catastrophic degeneration. Similar to the phenotype of *Sarm1*$^{-/-}$, injured *DR6*$^{-/-}$ axons showed formation of spheroids and spheroidal calcium accumulation (Fig. 4). Indeed, we've shown in the past that DR6 is also required for JNK activity after injury [25]. Because of our previous work examining the role of DR6 in trophic withdrawal induced degeneration, it is tempting to speculate that DR6 gates entry into the catastrophic phase WD [10]. SARM1 may play a similar role in gating entry into the catastrophic phase however, whether and how DR6 and SARM1 would work together to do this is unclear (Fig. 6).

Spheroid formation is a common hallmark for many neurodegenerative disorders including Alzheimer's disease (AD), glaucoma, amyotrophic lateral sclerosis (ALS) [33, 38, 58–60]. Our previous work suggests that these spheroids play a functional role as axons transition from latent to catastrophic phases of degeneration [10]. As such, understanding the regulation of these spheroids may help to rationalize therapeutic targets for a range of degenerative disorders.

Conclusion

This study demonstrates that: 1) severed sympathetic axons develop calcium rich spheroids and membrane ruptures prior to catastrophic degeneration. 2) Mechanistically, we show that sufficient NAD^+ pool is able to suppress the formation of axonal spheroids and delay WD after injury through a Rho-dependent pathway. 3) DR6 and SARM1 are unlikely to regulate spheroid formation, but may promote catastrophic degeneration downstream of spheroidal rupture. Based on our results and recent findings, we propose that 4) NMNAT degradation-dependent NAD^+ depletion contributes to spheroid formation, while SARM1 activation-dependent NAD^+ hydrolysis executes axon degeneration after spheroidal rupture in response to injury. Our findings contribute to further understanding of protective NAD^+ mechanisms in regulating the development of axonal spheroids that aid in the application of WD-blocking therapies for neurodegenerative disorders.

Abbreviations

NAD^+
Nicotinamide adenine dinucleotide
NMN
Nicotinamide mononucleotide
NMNAT
Nicotinamide mononucleotide adenylyltransferase
Nam
Nicotinamide
ATP
Adenosine triphosphate
ADPR
Adenosine diphosphate ribose
cADPR
Cyclic adenosine diphosphate ribose
WD
Wallerian degeneration
SARM1
Sterile alpha and TIR domain containing 1
DR6
Death receptor 6
WLD^s
Slow wallerian degeneration
DLK
Dual leucine zipper kinase
JNK
c-Jun N-terminal kinase
MAPK

Mitogen-activated protein kinase
ROS
Reactive oxygen species
SCG
Superior cervical ganglion
AD
Alzheimer's disease
ALS
Amyotrophic lateral sclerosis

Declarations

Ethical approval

All procedures for animal use were carried out in compliance with Association for Assessment of Laboratory Animal Care policies and approved by the University of Virginia Animal Care and Use Committee.

Consent for publication

We approve the manuscript for publication after acceptance.

Availability of data and materials

The raw datasets used and/or analyzed during current study are available from the corresponding author on reasonable request.

Competing interests

The authors declare no competing interests.

Funding

This study was supported by NIH-NINDS grant R01NS091617 and the Owens family foundation awarded to C.D.D.

Authors' contributions

YY proposed and designed the study. YY acquired all the data and interpreted the data. YY also wrote and revised the current manuscript. KG substantially contributed to designing and performing experiments to measure axon degeneration in microfluidic culture system. KG was also a major contributor to writing the manuscript. CC performed immunostaining and quantification of injured axons. AS contributed to designing the experiments to measure extracellular calcium in the conditioned media. CD provided funding for the study, and significantly contributed to the conception and design of the study. CD

significantly contributed to interpreting the data, writing and revising the manuscript. All authors read and approved the final manuscript.

Acknowledgements

We thank Pamela Neff for technical assistance. Austin Keeler, Sushanth Kumar, Shayla Clark, Amrita Pathak, Amy Van Deusen, Vitaly Zimyanin and Brandon Podyma for helpful discussions and comments on the manuscript. We thank Ammasi Periasamy and acknowledge the Keck Center for Cellular Imaging for the usage of the Leica SP5X microscopy system (NIH-RR025616). We wish to thank Genentech for kindly providing the *DR6*$^{-/-}$ mouse line.

Authors information

Department of Biology, University of Virginia, Charlottesville, VA, 22903, USA

Yu Yong, Anthony Spano & Christopher D. Deppmann

Department of Neuroscience, University of Virginia, Charlottesville, VA, 22903, USA

Courtny Cushman & Christopher D. Deppmann

Department of Stem Cell and Regenerative Biology, Harvard University, Cambridge, MA, 02138, USA

Kanchana Gamage

References

1. Waller A. Experiments on the Section of the Glosso-Pharyngeal and Hypoglossal Nerves of the Frog, and Observations of the Alterations Produced Thereby in the Structure of Their Primitive Fibres. Edinb Med Surg J. 1851;76:369–76.
2. Beirowski B, Adalbert R, Wagner D, et al. The progressive nature of Wallerian degeneration in wild-type and slow Wallerian degeneration (WldS) nerves. BMC Neurosci. 2005;6:6. doi:10.1186/1471-2202-6-6.
3. Wang JT, Medress ZA, Barres BA. Axon degeneration: molecular mechanisms of a self-destruction pathway. J Cell Biol. 2012;196:7–18. doi:10.1083/jcb.201108111.
4. Vargas ME, Yamagishi Y, Tessier-Lavigne M, Sagasti A. Live Imaging of Calcium Dynamics during Axon Degeneration Reveals Two Functionally Distinct Phases of Calcium Influx. J Neurosci. 2015;35:15026–38. doi:10.1523/JNEUROSCI.2484-15.2015.
5. Avery MA, Rooney TM, Pandya JD, et al. WldS prevents axon degeneration through increased mitochondrial flux and enhanced mitochondrial Ca2 + buffering. Curr Biol. 2012;22:596–600. doi:10.1016/j.cub.2012.02.043.

6. George EB, Glass JD, Griffin JW. Axotomy-induced axonal degeneration is mediated by calcium influx through ion-specific channels. J Neurosci. 1995;15:6445–52.
7. Adalbert R, Morreale G, Paizs M, et al. Intra-axonal calcium changes after axotomy in wild-type and slow Wallerian degeneration axons. Neuroscience. 2012;225:44–54. doi:10.1016/j.neuroscience.2012.08.056.
8. Yang J, Weimer RM, Kallop D, et al. Regulation of axon degeneration after injury and in development by the endogenous calpain inhibitor calpastatin. Neuron. 2013;80:1175–89. doi:10.1016/j.neuron.2013.08.034.
9. Ma M, Ferguson TA, Schoch KM, et al. Calpains mediate axonal cytoskeleton disintegration during Wallerian degeneration. Neurobiol Dis. 2013;56:34–46. doi:10.1016/j.nbd.2013.03.009.
10. Yong Y, Gamage K, Cheng I, et al. p75NTR and DR6 Regulate Distinct Phases of Axon Degeneration Demarcated by Spheroid Rupture. J Neurosci. 2019;39:9503–20. doi:10.1523/JNEUROSCI.1867-19.2019.
11. Saxena S, Caroni P. Mechanisms of axon degeneration: from development to disease. Prog Neurobiol. 2007;83:174–91. doi:10.1016/j.pneurobio.2007.07.007.
12. Llobet Rosell A, Neukomm LJ. Axon death signalling in Wallerian degeneration among species and in disease. Open Biol. 2019;9:190118. doi:10.1098/rsob.190118.
13. Coleman M. Axon degeneration mechanisms: commonality amid diversity. Nat Rev Neurosci. 2005;6:889–98. doi:10.1038/nrn1788.
14. Lunn ER, Perry VH, Brown MC, et al. Absence of Wallerian Degeneration does not Hinder Regeneration in Peripheral Nerve. Eur J Neurosci. 1989;1:27–33. doi:10.1111/j.1460-9568.1989.tb00771.x.
15. Brown MC, Lunn ER, Perry VH. Consequences of slow Wallerian degeneration for regenerating motor and sensory axons. J Neurobiol. 1992;23:521–36. doi:10.1002/neu.480230507.
16. Conforti L, Tarlton A, Mack TG, et al. A Ufd2/D4Cole1e chimeric protein and overexpression of Rbp7 in the slow Wallerian degeneration (WldS) mouse. Proc Natl Acad Sci USA. 2000;97:11377–82. doi:10.1073/pnas.97.21.11377.
17. Sasaki Y, Araki T, Milbrandt J. Stimulation of nicotinamide adenine dinucleotide biosynthetic pathways delays axonal degeneration after axotomy. J Neurosci. 2006;26:8484–91. doi:10.1523/JNEUROSCI.2320-06.2006.
18. Gilley J, Coleman MP. Endogenous Nmnat2 is an essential survival factor for maintenance of healthy axons. PLoS Biol. 2010;8:e1000300. doi:10.1371/journal.pbio.1000300.
19. Summers DW, Milbrandt J, DiAntonio A. Palmitoylation enables MAPK-dependent proteostasis of axon survival factors. Proc Natl Acad Sci USA. 2018;115:E8746–54. doi:10.1073/pnas.1806933115.
20. Walker LJ, Summers DW, Sasaki Y, et al. (2017) MAPK signaling promotes axonal degeneration by speeding the turnover of the axonal maintenance factor NMNAT2. elife. doi: 10.7554/eLife.22540.

21. Milde S, Gilley J, Coleman MP. Subcellular localization determines the stability and axon protective capacity of axon survival factor Nmnat2. PLoS Biol. 2013;11:e1001539. doi:10.1371/journal.pbio.1001539.
22. Osterloh JM, Yang J, Rooney TM, et al. dSarm/Sarm1 is required for activation of an injury-induced axon death pathway. Science. 2012;337:481–4. doi:10.1126/science.1223899.
23. Gerdts J, Brace EJ, Sasaki Y, et al. SARM1 activation triggers axon degeneration locally via NAD^+ destruction. Science. 2015;348:453–7. doi:10.1126/science.1258366.
24. Essuman K, Summers DW, Sasaki Y, et al. The SARM1 Toll/Interleukin-1 Receptor Domain Possesses Intrinsic NAD + Cleavage Activity that Promotes Pathological Axonal Degeneration. Neuron. 2017;93:1334–43.e5. doi:10.1016/j.neuron.2017.02.022.
25. Gamage KK, Cheng I, Park RE, et al. Death receptor 6 promotes wallerian degeneration in peripheral axons. Curr Biol. 2017;27:890–6. doi:10.1016/j.cub.2017.01.062.
26. Zhai Q, Wang J, Kim A, et al. Involvement of the ubiquitin-proteasome system in the early stages of wallerian degeneration. Neuron. 2003;39:217–25. doi:10.1016/S0896-6273(03)00429-X.
27. Larhammar M, Huntwork-Rodriguez S, Jiang Z, et al. (2017) Dual leucine zipper kinase-dependent PERK activation contributes to neuronal degeneration following insult. elife. doi: 10.7554/eLife.20725.
28. Yang J, Wu Z, Renier N, et al. Pathological axonal death through a MAPK cascade that triggers a local energy deficit. Cell. 2015;160:161–76. doi:10.1016/j.cell.2014.11.053.
29. Babetto E, Beirowski B, Russler EV, et al. The Phr1 ubiquitin ligase promotes injury-induced axon self-destruction. Cell Rep. 2013;3:1422–9. doi:10.1016/j.celrep.2013.04.013.
30. Murata H, Khine CC, Nishikawa A, et al. c-Jun N-terminal kinase (JNK)-mediated phosphorylation of SARM1 regulates NAD + cleavage activity to inhibit mitochondrial respiration. J Biol Chem. 2018;293:18933–43. doi:10.1074/jbc.RA118.004578.
31. Neukomm LJ, Burdett TC, Seeds AM, et al. Axon death pathways converge on axundead to promote functional and structural axon disassembly. Neuron. 2017;95:78–91.e5. doi:10.1016/j.neuron.2017.06.031.
32. Mi W, Beirowski B, Gillingwater TH, et al. The slow Wallerian degeneration gene, WldS, inhibits axonal spheroid pathology in gracile axonal dystrophy mice. Brain. 2005;128:405–16. doi:10.1093/brain/awh368.
33. Sasaki S, Warita H, Abe K, Iwata M. Impairment of axonal transport in the axon hillock and the initial segment of anterior horn neurons in transgenic mice with a G93A mutant SOD1 gene. Acta Neuropathol. 2005;110:48–56. doi:10.1007/s00401-005-1021-9.
34. Beirowski B, Nógrádi A, Babetto E, et al. Mechanisms of axonal spheroid formation in central nervous system Wallerian degeneration. J Neuropathol Exp Neurol. 2010;69:455–72. doi:10.1097/NEN.0b013e3181da84db.

35. Deppmann CD, Mihalas S, Sharma N, et al. A model for neuronal competition during development. Science. 2008;320:369–73. doi:10.1126/science.1152677.
36. Singh KK, Park KJ, Hong EJ, et al. Developmental axon pruning mediated by BDNF-p75NTR-dependent axon degeneration. Nat Neurosci. 2008;11:649–58. doi:10.1038/nn.2114.
37. Schindelin J, Arganda-Carreras I, Frise E, et al. Fiji: an open-source platform for biological-image analysis. Nat Methods. 2012;9:676–82. doi:10.1038/nmeth.2019.
38. Conforti L, Gilley J, Coleman MP. Wallerian degeneration: an emerging axon death pathway linking injury and disease. Nat Rev Neurosci. 2014;15:394–409. doi:10.1038/nrn3680.
39. Barsukova AG, Forte M, Bourdette D. Focal increases of axoplasmic Ca2+, aggregation of sodium-calcium exchanger, N-type Ca2 + channel, and actin define the sites of spheroids in axons undergoing oxidative stress. J Neurosci. 2012;32:12028–37. doi:10.1523/JNEUROSCI.0408-12.2012.
40. Hall A. Rho GTPases and the Actin Cytoskeleton. Science. 1998;279:509–14. doi:10.1126/science.279.5350.509.
41. Witte ME, Schumacher A-M, Mahler CF, et al. Calcium Influx through Plasma-Membrane Nanoruptures Drives Axon Degeneration in a Model of Multiple Sclerosis. Neuron. 2019;101:615–24.e5. doi:10.1016/j.neuron.2018.12.023.
42. Eddleman CS, Ballinger ML, Smyers ME, et al. Endocytotic formation of vesicles and other membranous structures induced by Ca2 + and axolemmal injury. J Neurosci. 1998;18:4029–41.
43. Di Stefano M, Nascimento-Ferreira I, Orsomando G, et al. A rise in NAD precursor nicotinamide mononucleotide (NMN) after injury promotes axon degeneration. Cell Death Differ. 2015;22:731–42. doi:10.1038/cdd.2014.164.
44. Wang J, Zhai Q, Chen Y, et al. A local mechanism mediates NAD-dependent protection of axon degeneration. J Cell Biol. 2005;170:349–55. doi:10.1083/jcb.200504028.
45. Sasaki Y, Nakagawa T, Mao X, et al. (2016) NMNAT1 inhibits axon degeneration via blockade of SARM1-mediated NAD + depletion. elife. doi: 10.7554/eLife.19749.
46. Gerdts J, Summers DW, Milbrandt J, DiAntonio A. Axon Self-Destruction: New Links among SARM1, MAPKs, and NAD + Metabolism. Neuron. 2016;89:449–60. doi:10.1016/j.neuron.2015.12.023.
47. Coleman MP, Höke A. Programmed axon degeneration: from mouse to mechanism to medicine. Nat Rev Neurosci doi. 2020. 10.1038/s41583-020-0269-3.
48. Sasaki Y, Engber TM, Hughes RO, et al. (2020) cADPR is a gene dosage-sensitive biomarker of SARM1 activity in healthy, compromised, and degenerating axons. Exp Neurol 113252. doi:10.1016/j.expneurol.2020.113252.
49. Guse AH. Calcium mobilizing second messengers derived from NAD. Biochim Biophys Acta. 2015;1854:1132–7. doi:10.1016/j.bbapap.2014.12.015.
50. Villegas R, Martinez NW, Lillo J, et al. Calcium release from intra-axonal endoplasmic reticulum leads to axon degeneration through mitochondrial dysfunction. J Neurosci. 2014;34:7179–89. doi:10.1523/JNEUROSCI.4784-13.2014.

51. Orem BC, Pelisch N, Williams J, et al. Intracellular calcium release through IP3R or RyR contributes to secondary axonal degeneration. Neurobiol Dis. 2017;106:235–43. doi:10.1016/j.nbd.2017.07.011.
52. Nikiforov A, Kulikova V, Ziegler M. The human NAD metabolome: Functions, metabolism and compartmentalization. Crit Rev Biochem Mol Biol. 2015;50:284–97. doi:10.3109/10409238.2015.1028612.
53. Mitchell L, Hobbs GA, Aghajanian A, Campbell SL. Redox regulation of Ras and Rho GTPases: mechanism and function. Antioxid Redox Signal. 2013;18:250–8. doi:10.1089/ars.2012.4687.
54. Heo J, Campbell SL. Mechanism of redox-mediated guanine nucleotide exchange on redox-active Rho GTPases. J Biol Chem. 2005;280:31003–10. doi:10.1074/jbc.M504768200.
55. Zhao ZY, Xie XJ, Li WH, et al. A Cell-Permeant Mimetic of NMN Activates SARM1 to Produce Cyclic ADP-Ribose and Induce Non-apoptotic Cell Death. iScience. 2019;15:452–66. doi:10.1016/j.isci.2019.05.001.
56. Wang Q, Zhang S, Liu T, et al. Sarm1/Myd88-5 Regulates Neuronal Intrinsic Immune Response to Traumatic Axonal Injuries. Cell Rep. 2018;23:716–24. doi:10.1016/j.celrep.2018.03.071.
57. Galindo R, Banks Greenberg M, Araki T, et al. NMNAT3 is protective against the effects of neonatal cerebral hypoxia-ischemia. Ann Clin Transl Neurol. 2017;4:722–38. doi:10.1002/acn3.450.
58. Adalbert R, Gilley J, Coleman MP. Abeta, tau and ApoE4 in Alzheimer's disease: the axonal connection. Trends Mol Med. 2007;13:135–42. doi:10.1016/j.molmed.2007.02.004.
59. Kanaan NM, Pigino GF, Brady ST, et al. Axonal degeneration in Alzheimer's disease: when signaling abnormalities meet the axonal transport system. Exp Neurol. 2013;246:44–53. doi:10.1016/j.expneurol.2012.06.003.
60. Howell GR, Libby RT, Jakobs TC, et al. Axons of retinal ganglion cells are insulted in the optic nerve early in DBA/2J glaucoma. J Cell Biol. 2007;179:1523–37. doi:10.1083/jcb.200706181.

Supplemental Information Note

Additional file 1: Dextran 3 kDa entry to axonal spheroids after injury

Live imaging of dextran 3 kDa (red) entry to axonal spheroids (black) 40 minutes after injury. Yellow empty arrows indicate that dextran 3 kDa entry to axonal spheroids at later time points. White filled arrows indicate spheroid moving and merging to form a bigger spheroid that eventually ruptured. No vesicular or punctate labeling was observed during dextran incubation, which is consistent with membrane rupture, instead of macropinocytosis. Scale bar = 10μm.

Figures

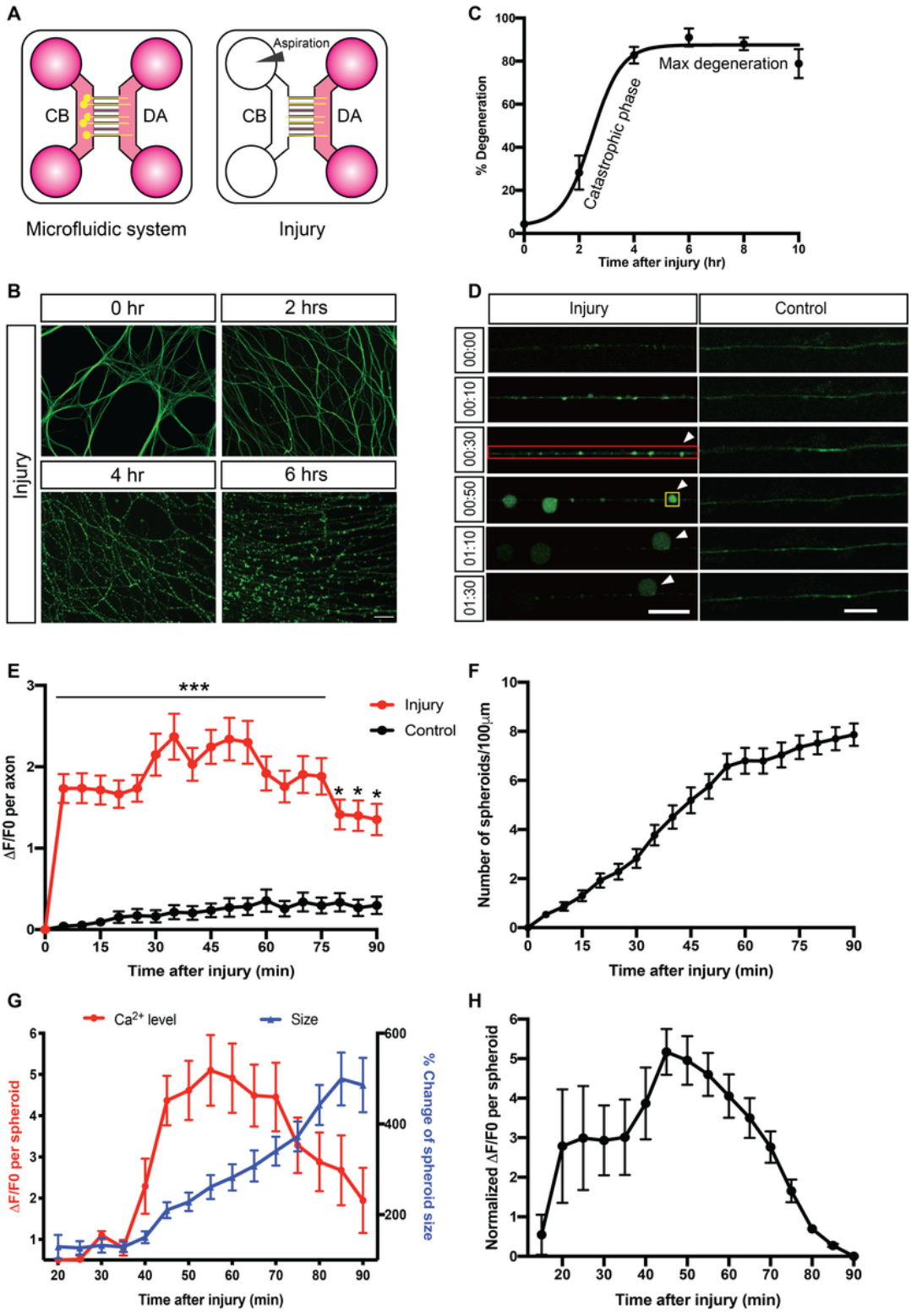

Figure 1

Axoplasmic calcium dynamics and formation of spheroids prior to catastrophic degeneration in response to injury (A) Schematic representation of injury paradigm in microfluidic devices. Cell bodies (CB) and distal axons (DA) are seperated. All the cultures were maintained in the presence of 45ng/mL NGF. For the “injury” condition, neurons were enucleated by aspiration in PBS. (B) Representative images of β3-tubulin immuno-stained distal sympathetic axons before treatment (0hr), 2, 4 and 6 hours after injury.

Scale bar = 50μm. (C) Degeneration time course after injury. Catastrophic phase and maximum of degeneration are noted. Nonlinear regression curve was drawn according to the Hill equation. n=3 for each time point. (D) Fluo4-AM calcium imaging of sympathetic axons at the indicated times after injury. For the “injury” condition, neurons were enucleated by aspiration in PBS and then incubated with Fluo4-AM for calcium imaging. For the “Control” condition, no injury was performed. Red box indicates the individual axon as a region of interest. Yellow box indicates axonal spheroid as a region of interest. White arrowheads indicate the formation and growth of spheroid. Scale bar = 10μm. (E) Calcium fluorescence change of control or injured axons over time. Total number of n=76 (injury) and n=30 (control) of axons from 3 independent litters were quantified. (F) Quantification of axonal spheroid number per 100μm of axon at the indicated times after injury. Total number of n=47 axons from 3 independent litters were counted. (G) Calcium fluorescence and size change of axonal spheroid at the indicated times after injury. Total number of n=14 axonal spheroids from 3 independent litters were quantified. (H) Quantification of normalized calcium fluorescence of axonal spheroids from 20 to 90 minutes after injury. Individual axonal spheroids were quantified: n=14 spheroids from 3 independent replicates. Data are reported as mean±SEM, *$p<0.05$, ***$p<0.0001$, two-way ANOVA with Sidak’s multiparisons test.

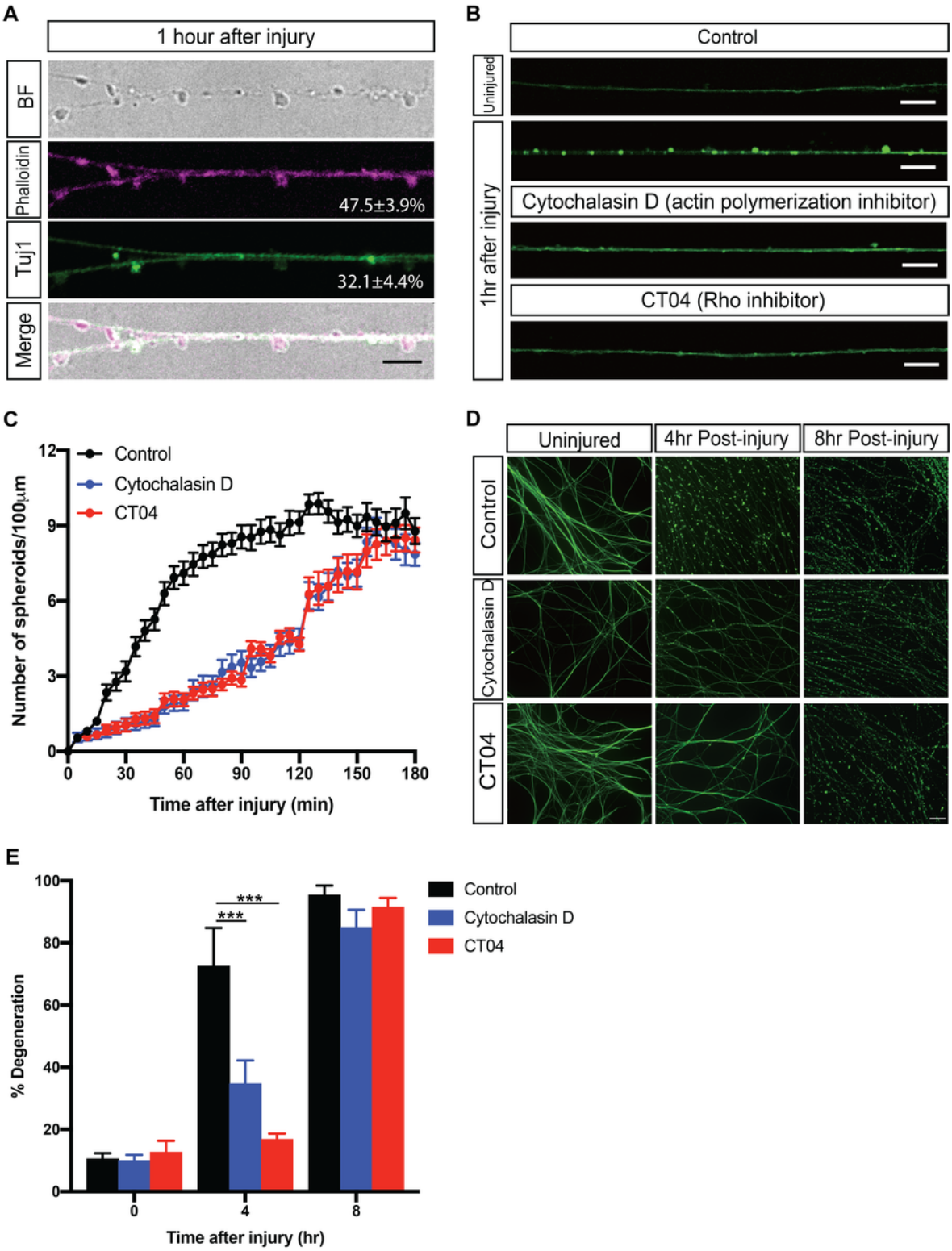

Figure 2

Rho activation and actin remodeling are required for axonal spheroid formation in response to injury (A) Representative axons/spheroids visualized for bright field, Phalloidin and β3-tubulin (Tuj1) 1 hour after injury. Scale bar = 5 μm. Percentages of Phalloidin positive and Tuj1 positive spheroids were quantified next to the images, respectively. Total number of n=10 axons were quantified. (B) Fluo4-AM calcium imaging of wild-type sympathetic axons with or without drug treatment. For the “CT04” group, wild-type

axons were incubated in SCG media containing 1μg/mL Rho inhibitor CT04, for 2 hours prior to injury. For the “Cytochalasin D” group, wild-type axons were incubated in SCG media containing 10μg/mL actin polymerization inhibitor for 2 hours prior to injury. Scale bar = 10μm. (C) Quantification of axonal spheroid number per 100μm of wild-type sympathetic axons at the indicated times after injury in the absence and presence of CT04 or Cytochalasin D. Total number of n=50 (Control), n=28 (Cytochalasin D), n=32 (CT04) axons from cultured neurons harvested from 3 independent litters were quantified. (D) Representative images and (E) quantification of degeneration of wild-type distal sympathetic axons immuno-stained for β3-tubulin in the absence and presence of CT04 or Cytochalasin D. Scale bar = 50μm. Compared to Control, 4hr post-injury (n=4), $p<0.0001$, n=6 for Cytochalasin D, 4hr post-injury; $p<0.0001$, n=5 for CT04, 4hr post-injury, two-way ANOVA with Dunnett’s multiple comparisons test. Data are reported as mean±SEM, *$p<0.05$, ***$p<0.0001$.

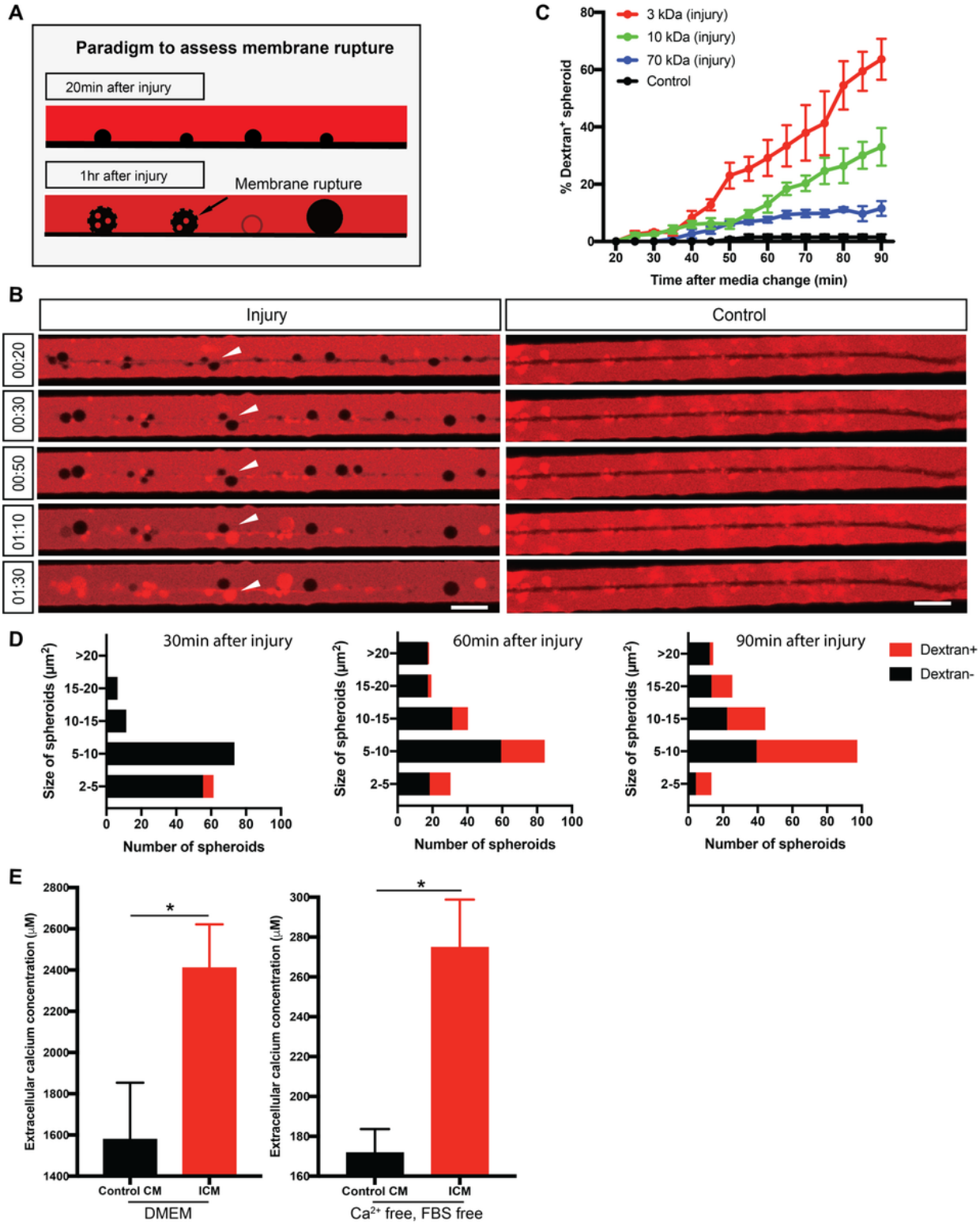

Figure 3

Axonal spheroids develop membrane rupture after injury (A) Schematic representation of the experimental paradigm to assess membrane rupture model using fluorescent dextran. 20 minutes after injury, fluorescent dextran (red) is not taken up by the axon (black, negative space). However, by 1 hour after injury, as the plasma membrane loses integrity and ruptures, fluorescent dextran (red) can diffuse into spheroids, turning them red. Spheroids with intact membrane remain black. (B) Representative

images of dextran 3 kDa (red) entry to axonal spheroids (black) from 20 to 90 minutes after injury (left column), and dextran exclusion in untreated axons (right column). White arrowheads indicate that dextran 3 kDa enter axonal spheroids 1 hour after injury. Scale bar = 10 μm. (C) Quantification of the percentages of fluorescent 3 kDa (red), 10 kDa (green), and 70 kDa (blue) dextran positive spheroids 20 to 90 minutes after injury. Black line (control) indicates the percentages of fluorescent 3 kDa dextran positive spheroids without injury. Total number of n=12 (3 kDa), n=12 (10 kDa), n=9 (70 kDa), and n=27 (control) axons from 3 independent litters were counted. (D) Histogram of 3 kDa dextran negative (black) and positive (red) spheroids 30, 60, and 90 minutes after injury. (E) Measurements of extracellular calcium expelled from axons into regular SCG culture media (DMEM, left) and calcium free, FBS free media (right). In the “Control CM” group, media was collected from uninjured axons. In the “ICM” group, media was collected 1 hour after injury. For DMEM groups, compared to Control CM (n=4), p=0.0414, n=4 for ICM; For calcium free, FBS free groups, compared to Control CM (n=3), p=0.0185, n=3 for ICM, unpaired t test. Data are reported as mean±SEM, *p<0.05, ***p<0.0001.

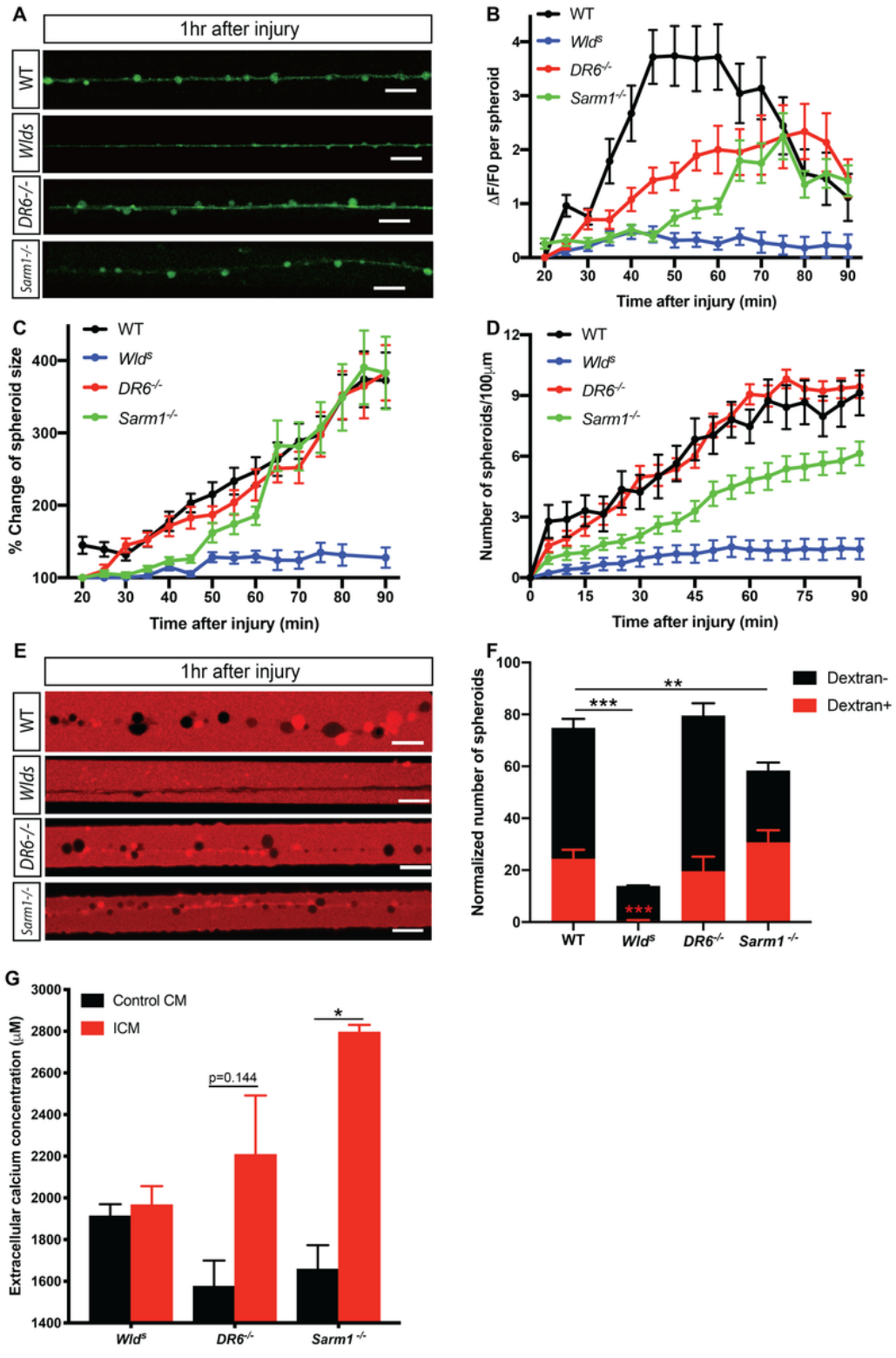

Figure 4

DR6-/- and Sarm1-/- develop axonal spheroids and spheroidal rupture after injury, while Wlds does not (A) Fluo4-AM calcium imaging of wild-type, Wlds, DR6-/-, and Sarm1-/- sympathetic axons 1hr after injury. Scale bar = 10μm. (B) Quantification of calcium level, (C) size change, and (D) numbers of axonal spheroids on the wild-type, Wlds, DR6-/-, and Sarm1-/- axons 1 hour after injury, respectively. Total number of n=29 (WT), n=17 (Wlds), n=57 for (DR6-/-), and n=54 (Sarm1-/-) axons from 3 independent

litters were counted. (E) Representative images of dextran 3 kDa (red) entry to axonal spheroids (black) on wild-type, Wlds, DR6-/-, and Sarm1-/- axons 1 hour after injury. Scale bar = 10μm. (F) Normalized numbers of 3 kDa dextran negative (black) and positive (red) axonal spheroids on wild-type, Wlds, DR6-/-, and Sarm1-/- axons 1 hour after injury. Compared to WT, Dextran+, $p<0.0001$, n=21 for Wlds, Dextran+. Compared to WT, Dextran-, $p<0.0001$, n=22 for Wlds, Dextran-; $p=0.0003$, n=17 for Sarm1-/-, Dextran-, two-way ANOVA with Dunnett's multiple comparisons test. (G) Measurement of extracellular calcium concentration in media surrounding injured and uninjured Wlds, DR6-/- and Sarm1-/- axons. All injured conditioned media was collected from distal axon chamber 1hr after injury. Compared to Control CM, $p=0.9982$, n=3 for Wlds, ICM; $p=0.1440$, n=6 for DR6-/-, ICM; $p=0.0141$, n=3 for Sarm1-/-, ICM, two-way ANOVA with Sidak's multiple comparisons test. Data are reported as mean±SEM, *$p<0.05$, **$p<0.001$, ***$p<0.0001$.

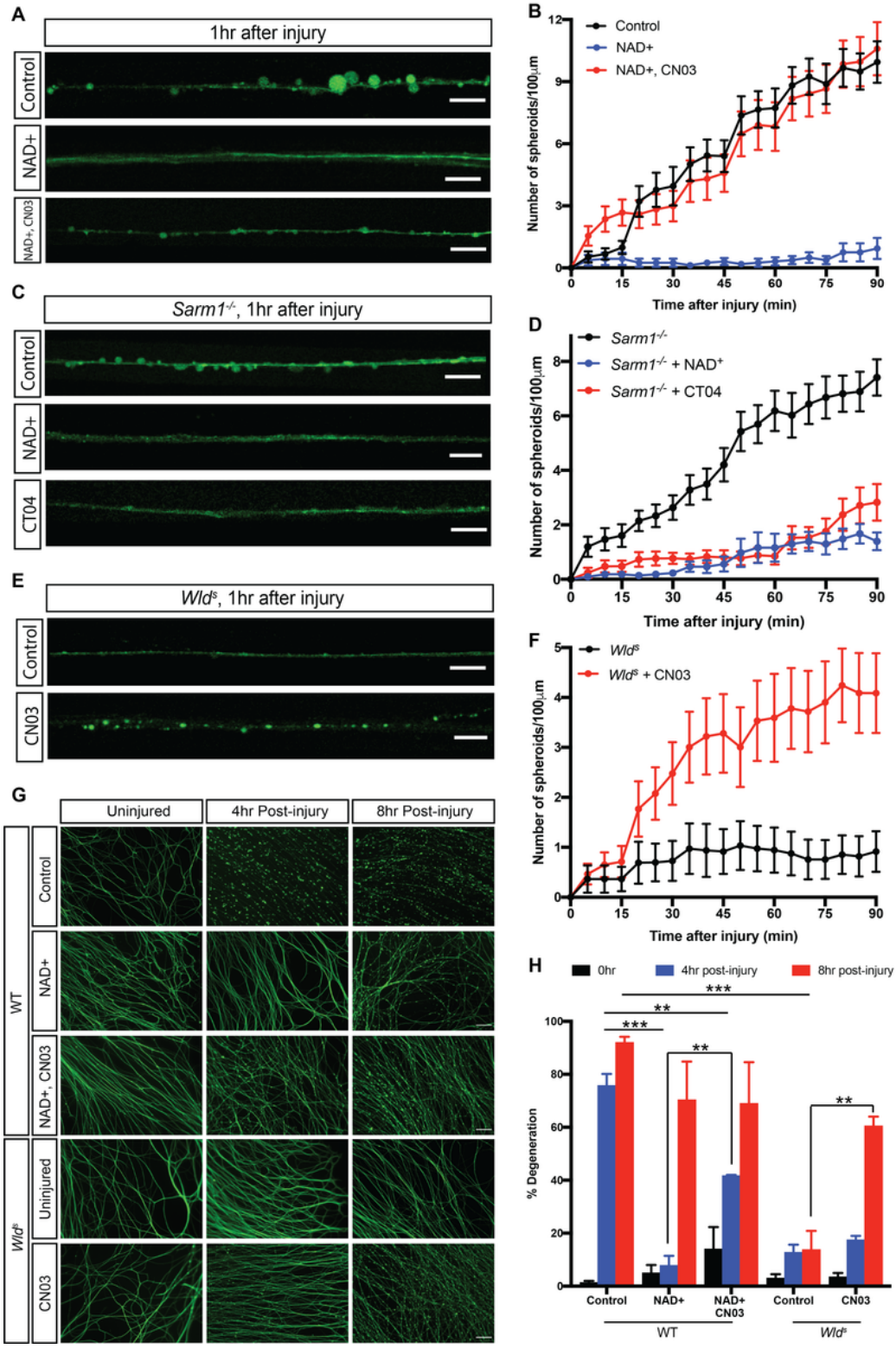

Figure 5

NAD+ acts on upstream of Rho activation to suppresses spheroid formation after injury (A) Fluo4-AM calcium imaging of wild-type sympathetic axons 1hr after injury with or without drug treatment. Scale bar = 10μm. (B) Quantification of axonal spheroid number per 100μm of wild-type sympathetic axons at the indicated times after injury in the absence and presence of NAD+ or CN03. Total number of n=23 (Control), n=13 (NAD+), n=21 (NAD+, CN03) axons from cultured neurons harvested from 3 independent

litters were quantified. (C) Fluo4-AM calcium imaging of Sarm1-/- sympathetic axons 1hr after injury with or without drug treatment. Scale bar = 10μm. (D) Quantification of axonal spheroid number per 100μm of Sarm1-/- sympathetic axons at the indicated times after injury in the absence and presence of NAD+ or CT04. Total number of n=30 (Control), n=16 (NAD+), n=25 (CT04) Sarm1-/- axons from cultured neurons harvested from 3 independent litters were quantified. (E) Fluo4-AM calcium imaging of Wlds sympathetic axons 1hr after injury in the presence and absence of CN03. Scale bar = 10μm. (F) Quantification of axonal spheroid number per 100μm of Wlds sympathetic axons at the indicated times after injury in the absence and presence of CN03. Total number of n=25 (Control), n=24 (CN03) Wlds axons from cultured neurons harvested from 3 independent litters were quantified. (G) Representative images and (H) quantification of degeneration of wild-type and Wlds distal sympathetic axons immuno-stained for β3-tubulin with different treatments. Scale bar = 50μm. For the "NAD+" group, axons were incubated in SCG media containing 1mM NAD+ supplement overnight prior to injury. For the "CN03" and CT04" groups, axons were incubated in SCG media containing 1μg/mL Rho activator CN03 and Rho inhibitor CT04 for 2 hours prior to injury, respectively. Data are reported as mean±SEM, *p<0.05, **p<0.001, ***p<0.0001, two-way ANOVA with Tukey's multiple comparisons test.

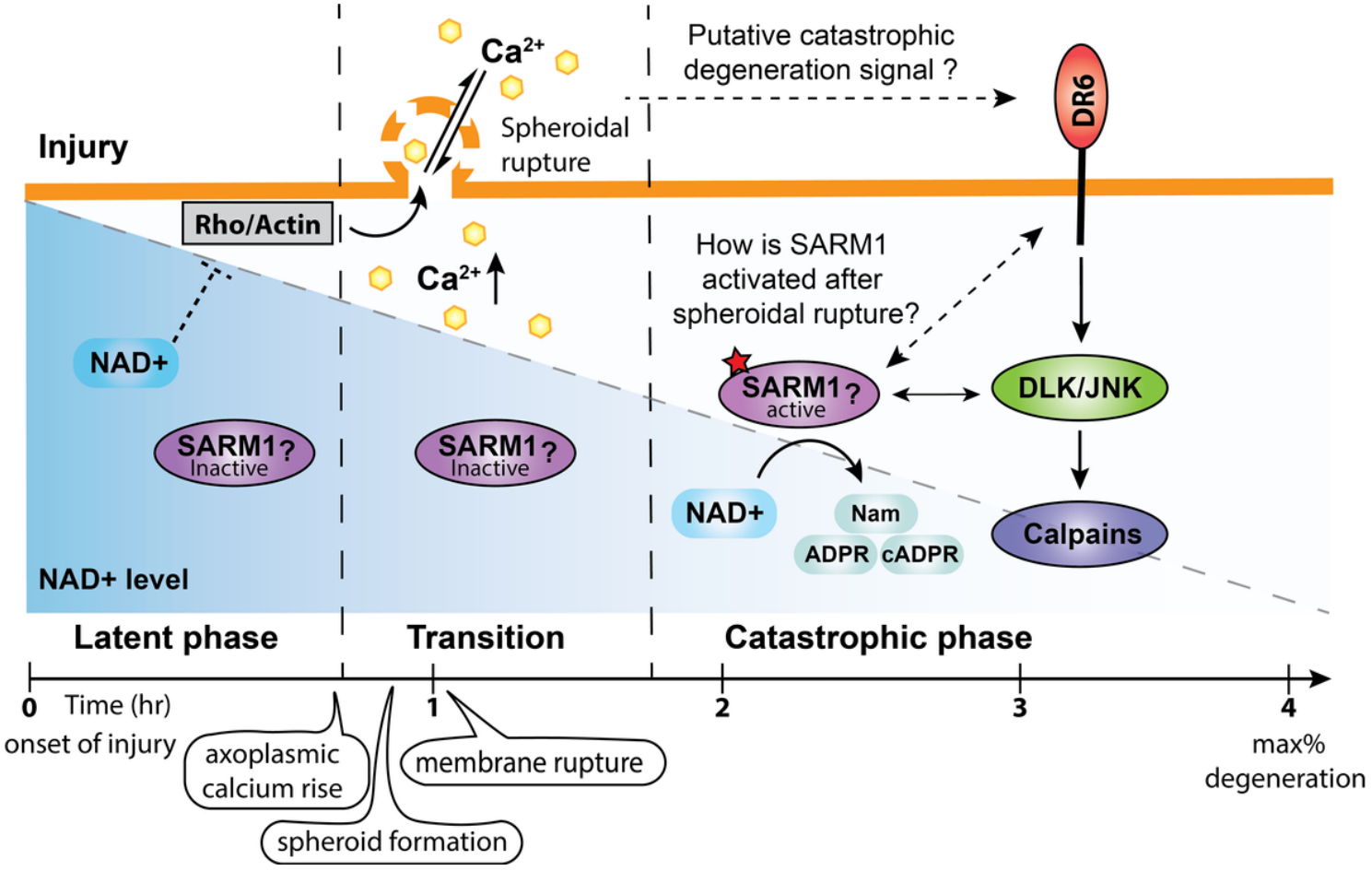

Figure 6

Proposed model for events associated with injury induced axon degeneration of sympathetic neurons After injury, axoplasmic calcium is increased and enriched in spheroids prior to catastrophic phase. Spheroid formation is regulated by Rho activity and actin remodeling, which is suppressed by NAD+. The

calcium electrochemical gradient across membrane is disrupted by spheroidal rupture. We speculate that axonal NAD+ level decreases via SARM1 independent catalysis while SARM1 stays inactive prior to spheroidal rupture. DR6 and SARM1 can be activated to promote further NAD+ depletion and catastrophic degeneration.

Supplementary Files

This is a list of supplementary files associated with this preprint. Click to download.

- Additionalfile1.mp4